Biogeosciences Discuss., 12, 4557–4593, 2015
www.biogeosciences-discuss.net/12/4557/2015/
doi:10.5194/bgd-12-4557-2015

Biogeosciences Discussions
Open Access

Can organic matter flux profiles be diagnosed using remineralisation rates derived from observed tracers and modelled ocean transport rates?

J. D. Wilson[1,2], **A. Ridgwell**[2,3], **and S. Barker**[1]

[1]School of Earth and Ocean Sciences, Cardiff University, Cardiff, UK
[2]School of Geographical Sciences, University of Bristol, UK
[3]Department of Earth Sciences, University of California, Riverside CA, USA

Received: 2 March 2015 – Accepted: 3 March 2015 – Published: 19 March 2015

Correspondence to: J. D. Wilson (wilsonjd@cardiff.ac.uk)

Published by Copernicus Publications on behalf of the European Geosciences Union.

Abstract

The average depth in the ocean at which the majority of sinking organic matter particles remineralise is a fundamental parameter in the oceans role in regulating atmospheric CO_2. Observed spatial patterns in sinking fluxes and relationships between the fluxes of different particles in the modern ocean have widely been used to invoke controlling mechanisms with important implications for CO_2 regulation. However, such analyses are limited by the sparse spatial sampling of the available sediment trap data. Here we explore whether model ocean circulation rates, in the form of a transport matrix, can be used to derive remineralisation rates and sinking particle flux curves from the much more highly resolved observations of dissolved nutrient concentrations. Initially we use the Earth system model GENIE to generate a synthetic tracer dataset to explore the methods and its sensitivity to key sources of uncertainty arising from errors in the tracer observations and in the model circulation. We use a perturbed physics ensemble to generate 54 different estimates of circulation to explore errors associated with model transport rates. We find that reconstructed remineralisation rates are highly sensitive to both errors in observations and our ensemble uncertainty in model circulation rates such that a simple inversion does not provide a robust estimate of particulate flux profiles. Inferred remineralisation rates are particularly sensitive to differences between the "observed" and modelled transport fluxes because remineralisation rates are 3–4 magnitudes smaller than circulation rates. We also find that when inferring particle flux curves from remineralisation rates the cycling of dissolved organic matter also creates biases that have a similar magnitude and spatial variability to flux curves diagnosed using sediment trap data. We end with a discussion on the potential future directions and pitfalls of estimating remineralisation rates using model circulation schemes.

BGD
12, 4557–4593, 2015

1 Introduction

Sediment trap studies show that the vertical flux of particulate organic carbon (POC) can be described empirically by a power-law curve (e.g. the "Martin Curve" Martin et al., 1987; see Fig. 1a) where POC is rapidly remineralised in the upper water column (< 1000 m) leaving a small fraction (5–10 %) of POC that sinks to greater depths. The exponent of the Martin Curve (b) reflects the distribution of POC with depth and whether POC is remineralised higher or lower in the water column. Recent studies using global sediment trap observations, ^{234}Th fluxes and particle concentration data suggest a highly heterogeneous pattern of flux profiles and the existence of a general latitudinal trend (Lutz et al., 2007; Honjo et al., 2008; Lam et al., 2011; Henson et al., 2012). POC fluxes in high latitude regions decrease faster with depth, i.e. they display shallower flux curves than in low latitude regions where a greater proportion of POC is remineralised at deeper depths (Fig. 1a). These patterns may be biased by a focus on deep ocean fluxes however (Marsay et al., 2015). Analysis of the POC fluxes supports a number of mechanisms that explain these spatial patterns including increased sinking velocity of particles via a "ballast" effect from minerals such as $CaCO_3$ (Armstrong et al., 2002; Klaas and Archer, 2002); aggregation of particles (Passow, 2004); and surface ecosystem dynamics, such as the level of nutrient recycling and blooms altering characteristics of the particles being exported (Lam et al., 2011; Le Moigne et al., 2012; Henson et al., 2012). However, further progress has been hindered by the relatively low sampling density of long-term sediment trap deployments, particularly in regions such as the Southern Ocean, e.g. Le Moigne et al. (2012); Wilson et al. (2012).

Understanding the underlying reasons for the spatial patterns in remineralisation is a valuable step in understanding mechanisms driving the biological pump. This is key to understanding how the biological pump will respond to both past and current changes in climate (Honjo et al., 2014). Atmospheric carbon dioxide (CO_2) concentrations have been shown to be sensitive to changes in flux profiles when modelled, primarily via the effect of redistributing DIC in the modern ocean interior (Kwon et al., 2009). Atmo-

BGD
12, 4557–4593, 2015

spheric CO_2 is also potentially sensitive to changes in the POC flux to deep-sea sediments relative to fluxes of calcium carbonate ($CaCO_3$) over longer timescales (Archer and Maier-Reimer, 1994; Roth et al., 2014). The range of potential mechanisms results in a range of potential feedbacks for the biological pump of different magnitudes and directions that will respond to a range of different environmental factors. An additional source of uncertainty in modelling sensitivity studies is that only global changes in remineralisation depths, not spatially variable changes, have been considered.

A potential approach to increasing and enhancing the resolution of POC observations is to use climatological fields of dissolved nutrients to estimate remineralisation rates. The water column profile of remineralisation rates can be related to flux curves by the fact that the vertical profile of remineralisation rates is the first derivative of the vertical profile of fluxes (Fig. 1a and b). The global distribution of a biological nutrient, such as phosphate (PO_4) or dissolved inorganic carbon (DIC), results from the net action of the biological pump (uptake during photosynthesis at the ocean surface and subsequent remineralisation of organic matter in the interior) in combination with physical processes (e.g. air–sea gas exchange) and other biological processes (such as denitrification) that are integrated through time via ocean circulation. In particular, the concentration of Apparent Oxygen Utilisation (AOU) has a long history of use as a measure of net organic matter remineralisation in the ocean interior. When combined with a tracer tracking the age of water masses, AOU can be converted to apparent oxygen utilisation rates (AOUR) and related to carbon remineralisation via stoichiometric ratios, e.g. Jenkins (1982). Feely et al. (2004) compiled AOUR-derived profiles of organic carbon remineralisation rates for 10 regions in the Pacific noting higher rates in the North Pacific relative to the South Pacific and similarities between regions with high rates and higher $CaCO_3$ fluxes. However, the in-situ AOUR of a water parcel reflects the history of remineralisation over its whole trajectory (e.g. along an isopycnal) producing an average AOUR that is biased towards shallower regions where remineralisation rates are higher. Therefore, when relating AOURs back to flux profiles by integrating

BGD
12, 4557–4593, 2015

them vertically, estimates are representative of large oceanic regions only, i.e. there is a high degree of spatial smoothing (Sonnerup et al., 2013; Stanley et al., 2012).

An alternative to combining AOU and age tracers is to use the spatial gradients in tracers to separate out and quantify the change in a concentration of a tracer at any point from circulation only. Spatial gradients of a tracer along the trajectory of a water mass in the ocean interior reflect mixing with other water masses and processes such as the remineralisation of organic matter. Gradient based approaches aim to solve for the effect of mixing by defining a water mass as the sum of mass fractions from different sources, e.g. Anderson and Sarmiento (1994); Broecker et al. (1998); Gebbie and Huybers (2010). A recent development of this method, the Total Matrix Intercomparison (TMI) method described by Gebbie and Huybers (2010), solves for up to 6 mass fractions for each grid-box in a $4^{\circ} \times 4^{\circ}$ resolution with 33 vertical levels using temperature, salinity, $\delta^{18}O$, and nutrients with an additional source term reflecting organic matter remineralisation. The source term is related to the nutrients using stoichiometric ratios. The TMI method therefore produces a high resolution field of remineralisation estimates. However, these terms do not reflect a rate, i.e. TMI predicts mol PO_4 remineralised in a grid box rather than mol PO_4 yr^{-1}. This is because the TMI method reflects the pathways of ocean transport but not the rates of transport (Gebbie and Huybers, 2010).

Spatial gradients in tracers have also been used to diagnose export fluxes of calcium carbonate (Sarmiento et al., 2002) and opal (Sarmiento et al., 2004) from the surface. The method is based on taking the ratio between the vertical gradients of Alkalinity and Nitrate in the upper ocean, to reflect the $CaCO_3$: Organic Carbon export ratio assuming a dominance of vertical gradients (Sarmiento et al., 2002). The ratio is converted to a flux using estimates of organic carbon export e.g. Henson et al. (2011). However, a model-based assessment of the method suggests that biases could occur due to the remineralisation of dissolved organic matter (DOM) and strong meridional transports that violate the assumption of processes occurring primarily in the vertical dimension (Jin et al., 2006).

BGD
12, 4557–4593, 2015

Ocean circulation models offer the opportunity to estimate remineralisation rates of organic matter from tracer data by exploiting the calculated modelled transport rates to account for the effects of ocean circulation on tracers. The aim of this paper is to explore the feasibility of inferring flux profiles of particulate organic matter from remineralisation rates that have been derived from observed tracers. A method and example of estimating remineralisation rates using transport matrices is first introduced. We identify potential sources of error for this method. We then derive a set of model experiments that are used as a synthetic dataset with which to test the sensitivity of the approaches to various sources of error. Finally, we explore the uncertainties associated with the broader concept of inferring flux curves from remineralisation rates.

2 Estimating remineralisation rates using modelled ocean transport rates

Remineralisation rates can be calculated as the amount of tracer needed to maintain tracer observations at steady state once the effects of model ocean transport have been accounted for, i.e. transport divergence (Deutsch et al., 2007). Remineralisation rates can then be used to estimate the vertical particulate flux curve. A practical method for this approach is to apply a transport matrix approach. A transport matrix, hereafter abbreviated to TM, is a representation of steady state transport rates in the form of a sparse matrix that is derived empirically from an ocean circulation model (Khatiwala et al., 2005; Khatiwala, 2007). Using a TM is akin to the fixed transport rates implied in a box model, e.g. "LOSCAR": Zeebe (2012), but with the advantage that the rates are diagnosed from a dynamic ocean model with a much higher spatial resolution.

For every grid-box in the model the TM defines a set of fluxes of a tracer in and out of neighbouring grid-boxes due to ocean circulation during a single time-step of the model (see Table 1 for an illustrative example). Using the TM in place of the model circulation, the evolution of a tracer in time is then:

$$\boldsymbol{c}^{t+1} = \mathbf{A}\boldsymbol{c}^{t} + \boldsymbol{q} \quad (1)$$

BGD
12, 4557–4593, 2015

where **A** is the TM, $\boldsymbol{c}$ is a vector representation of the gridded three-dimensional tracer field (e.g. mol kg^{-1}) with the superscript referring to the time-step. $\boldsymbol{q}$ is a vector representation of any non-circulation related sources and/or sinks for a tracer (e.g. mol kg^{-1} dt^{-1}), for instance, due to remineralisation. Assuming steady state, the simplest approach to estimating remineralisation rates using Eq. (1) is to solve for $\boldsymbol{q}$ directly, given the TM and a steady state tracer. To achieve this practically, we use a related equation that uses the identity function (**I**) (see also Table 1 for role of **I**):

$$\frac{\mathrm{d}\boldsymbol{c}}{\mathrm{d}t} = (\mathbf{A} - \mathbf{I})\boldsymbol{c} + \boldsymbol{q} \tag{2}$$

Equation (2) can then be solved for $\boldsymbol{q}$ by assuming $\frac{\mathrm{d}\boldsymbol{c}}{\mathrm{d}t} = 0$, i.e. as assuming steady-state:

$$\boldsymbol{q} = -(\mathbf{A} - \mathbf{I})\boldsymbol{c} \tag{3}$$

Applying Eq. (3) with a steady-state tracer field is the same as initialising an ocean circulation model with observed tracer concentrations and then stepping the model forward for one time step. $\boldsymbol{q}$ will therefore reflect the exact interior source/sink terms needed in one time step to maintain the steady state tracer concentrations given the model transport rates. We refer to $\boldsymbol{q}$ as the interior source/sink (ISS) although it is not necessarily representing a mechanistic process.

2.1 Example using a general circulation model transport matrix

As an example of the approach, we use the annual average TM derived from a 2.8° configuration of the MITGCM model (available online: http://www.ldeo.columbia.edu/~spk/) to invert a regridded annual climatogical [PO_4] field (World Ocean Atlas 2009; Garcia et al., 2010), using Eq. (3) (Fig. 2). The resulting ISS estimates at shallower depths of the ocean interior (85 m) show some spatial patterns that are consistent with expectations of general export patterns, such as higher rates in the equatorial upwelling regions, and the subpolar regions of the Southern Ocean (Henson et al., 2011) (Fig. 2a).

BGD
12, 4557–4593, 2015

However, negative ISSs also exist, indicating a sink of PO_4, such as in regions of the subpolar Southern Ocean and Pacific equatorial upwelling. At deeper depths (2030 m) the elevated values in the Southern Ocean match the shallower pattern, but overall there are fewer clear spatial features and a more random pattern of positive and negative ISSs (Fig. 2b). The existence of so many negative values gives rise to near-zero values when averaging over large spatial scales.

Vertical profiles of the PO_4 ISSs show a range of features (Fig. 2c). Several show negative values at the surface, which is expected given this will reflect uptake of $[PO_4]$ by phytoplankton during photosynthesis. The Pacific profile at 35.17° S is smooth and fitting expectations of a remineralisation curve in Fig. 1c. The profile at 4.22° N however shows increasingly negative ISSs at shallower depths. This example shows that a simple inversion of $[PO_4]$ observations using this approach is susceptable to large errors that will likely hinder their interpretation.

3 Methods

3.1 Model description

To explore the errors when using modelled transport rates, we first derive a synthetic dataset using the Earth System model "GENIE" (Ridgwell et al., 2007a). GENIE features a 3-D ocean circulation model coupled to a 2-D energy-moisture balance model of the atmosphere and a dynamic-thermodynamic sea-ice model (Edwards and Marsh, 2005). In the configuration used here, the ocean model is non-seasonally forced and solved on a simplified 36 × 36 equal area horizontal grid (10° longitude by 3–15° latitude) with 8 vertical layers. The biogeochemical model is that described in Ridgwell et al. (2007a).

Our choice of GENIE over other possible models and available transport matrices reflects a number of considerations. The configuration of GENIE used here was derived using a perturbed-physics ensemble, where combinations of parameters relevant to the

BGD
12, 4557–4593, 2015

physical circulation were sampled to test the sensitivity of assumptions about ocean circulation and find an optimal set of parameters (Annan et al., 2005). The availability of this ensemble enables us to explore errors associated with uncertainty in model circulation states. The annual average circulation, coarse resolution and integration speed of GENIE also facilitate the relatively easy and fast retrieval of TMs. This is the first time that transport matrices have been constructed from an Earth system model. The relative simplicity of GENIE also keeps a focus on the methodological concept. It is worth noting that much of this could also be achieved by "coarse-graining" a TM derived from a higher resolution model, described in Khatiwala (2007), but without the availability of alternative circulation states.

3.2 Diagnosing transport matrices in GENIE

The method of Khatiwala et al. (2005) is adapted to diagnose a steady state ocean circulation simulation in GENIE. The *n*th ocean grid-box in GENIE is dyed with 1 mol kg^{-1} of an inert "colour" tracer. After the model is integrated for one time-step the resulting pattern of tracer is recovered, vectorised, and forms the *n*th column of a 6210 × 6210 sparse matrix. This is repeated for all 6210 ocean grid-boxes in GENIE. Our method of diagnosing the TM in GENIE differs from that detailed by Khatiwala et al. (2005) in two ways. First, we do not use smoother basis vectors and instead use the simpler method of dying a single grid-box. Secondly, each grid-box is initialised only once and there is no averaging because the circulation in the 8 level version of GENIE is annual average, i.e. non-seasonal. The circulation can therefore be diagnosed during a single continuous simulation.

3.3 Experiment design

We use the biogeochemical model described in Ridgwell et al. (2007a) with the biogeochemical parameter values described in Ridgwell et al. (2007b) to produce a synthetic dataset of tracers. In this, nutrients are utilised by biological activity in the sur-

BGD
12, 4557–4593, 2015

face ocean grid-boxes based on a nutrient and light limited scheme. A fraction of the uptake is exported from the surface as DOM which is advected and remineralised. The remaining fraction is exported (34 %) as particulate organic matter (POM) which remineralises instantaneously at depth according to the Martin Curve with a global b value of −0.858. The use of a Martin Curve keeps the discussion relevant to its use with sediment trap data and is the only difference between our model set-up and that of Ridgwell et al. (2007a, b). POM remaining in the deepest grid-box is completely remineralised to maintain a closed system, i.e. there are no sediment interactions.

3.3.1 Synthetic datasets

$[PO_4]$ is used as the tracer for inversion by the TM. An alternative tracer for this could be AOU (related to PO_4 via stoichiometric ratios), as this tracks only organic matter remineralisation (regenerated PO_4) whilst total phosphate also includes phosphate that has been advected from the surface (preformed PO_4). However, AOU is subject to assumptions about oxygen saturation (Ito et al., 2004; Duteil et al., 2013) and may also reflect non-biological processes (Dietze and Oschlies, 2005). To focus on errors deriving only from the method of inverting tracers, we choose to use $[PO_4]$ over AOU. We compare our TM derived estimates of PO_4 remineralisation with the total remineralisation of phosphate in each grid-box as diagnosed within the experiment run as mol PO_4 kg^{-1} $year^{-1}$ and is converted to dt^{-1} by dividing by the number of timesteps per year (96; dt = 0.01 year). The $[PO_4]$ field is the annual average taken from the last year of a 10 000 year spin-up. A corresponding TM is diagnosed at the end of the 10 000 year run. This synthetic dataset is referred to as SYN (Table 2). A second synthetic dataset (SYN-NODOM) is also produced in the same way as the SYN dataset except no DOM is produced to explore the effect of DOM when inferring flux curves from remineralisation rates.

BGD
12, 4557–4593, 2015

3.3.2 Experiments

We design a number of experiments to explore the sensitivity of the approach to various sources of error (experiment names are indicated in brackets and also described in Table 2):

1. (TWIN) We first use the TM corresponding to the synthetic dataset (SYN) to estimate remineralisation rates from the corresponding [PO_4] field as a proof of concept of the method (a twin-test).

2. (ERR-OBS) The effect of errors from the tracer observations themselves is simulated by calculating 100 random perturbations to the synthetic PO_4 concentrations (SYN) within one SD. For each grid-box, the mean is taken as the synthetic PO_4 concentration (SYN), and one SD from the SD of WOA [PO_4] observations regridded to the GENIE grid (Garcia et al., 2010).

3. (ERR-CIRC) To explore the effect of circulation uncertainty, we diagnose 54 individual TMs from an existing perturbed physics ensemble (Annan et al., 2005). The ensemble is the result of tuning circulation parameters to fit modern temperature and salinity fields using an ensemble Kalman filter. Each ensemble member is spun-up for 10 000 years after which the TM is diagnosed and used to invert the synthetic [PO_4] field (SYN). The circulation parameters in Ridgwell et al. (2007a, b) are an average of the ensemble parameters, such that the 54 TMs offer a range of different ocean circulation states. Details of the ensemble parameters and comparisons against the standard configuration can be found in the Supplement.

4. (ERR-DOM) We explore the effect of DOM when inferring particulate flux curves from remineralisation rates. As a comparison to the synthetic dataset, we run an identical experiment but with no DOM created (SYN-NODOM), i.e. all PO_4 is exported as particulate organic matter.

BGD
12, 4557–4593, 2015

4 The transport matrix inversion method

4.1 Assessment of the transport natrix inversion method

We use the output from GENIE as a synthetic dataset from which to assess the transport matrix inversion method and identify the sources and nature of the errors involved. Figure 3a and b show the [PO_4] field in GENIE at two depths, directly below the surface (290 m) and in the deep ocean (2106 m), with the corresponding annual average input of PO_4 from the continual remineralisation of sinking particles and dissolved organic matter at the same depths (Fig. 3c and d). The higher remineralisation values calculated for single grid-boxes occur where the remaining particulate flux is remineralised at the seafloor to maintain a closed system, i.e. to ensure there are no losses to sediments (Fig. 3d). We also show the inventory of phosphorus in DOM integrated over the ocean interior below 175 m (Fig. 3e). DOM has a visually similar pattern to shallow PO_4 remineralisation, because they are both linked by export production. The close resemblance and magnitude of the DOM at shallow depths may have implications for using remineralisation rates to infer remineralisation fluxes which will be discussed in Sect. 5. Finally, we note a correspondence between areas in the Southern Ocean with a large magnitude of remineralisation at shallow depths and locations where convection occurs in the model (Fig. 3f). This is consistent with high productivity driven by nutrients delivered to the surface via strong vertical mixing.

4.1.1 Twin-test

To demonstrate and test the method described in Sect. 2, we first invert the model generated synthetic [PO_4] field using the corresponding TM as per Eq. (3) (Fig. 4a). The interior source/sink term (ISS) calculated by inverting the synthetic [PO_4] field is consistent with the model calculated remineralisation with minor deviations from the 1 : 1 ratio line (Fig. 4a). This demonstrates the success of the approach as the errors in the synthetic tracer field and circulation scheme are effectively reduced to near-zero

BGD
12, 4557–4593, 2015

in this example. The errors between estimated and modelled remineralisation rates cluster around zero with a median proportion of error of 1.1×10^{-3} (Fig. 4b). Some larger errors, i.e. the outliers to the 1 : 1 line in Fig. 4a, occur in distinct regions such as in the shallow sub-tropics (Fig. 4e) and the deep equatorial Atlantic (Fig. 4f). These errors likely represent either, small differences in the circulation at individual time-steps that have been sampled by our method of sequentially dying grid-boxes during a single run, or are a result of the model circulation not being in strict steady state. Overall however the TM inversion of the synthetic [PO_4] estimates the PO_4 remineralisation rates very well (Fig. 4e and f c.f. Fig. 3c and d) with minor errors. This demonstrates that, in theory at least, modelled circulation rates in the form of a transport matrix can be used to successfully estimate remineralisation rates from a tracer field.

4.2 Sensitivity of inversions to sources of errors

Although remineralisation rates can be estimated by applying transport rates to a tracer field as shown above, there are several assumptions that will introduce error when this is applied to observations. In the following sections, we detail the results of experiments designed to explore these sources of error.

4.2.1 Error from observations

Error related to the 1° World Ocean Atlas annual mean climatology (Garcia et al., 2010) will introduce some uncertainty in the TM inversion due to measurement errors and biases in the climatology itself as well as re-gridding the observations onto a model grid such as GENIE or MITGCM. As a measure of how sensitive the TM inversion method is to these errors, we regrid the SD of annual [PO_4] observations onto the GENIE grid (Fig. 5). The SDs in each grid-box are used to produce an illustrative estimate of the uncertainty inherent in the observations. The SDs are highest in the coastal regions and high latitudes, and at shallower depths (Fig. 5a c.f. b).

BGD
12, 4557–4593, 2015

The SDs are used to produce 100 versions of the synthetic [PO_4] field that have been perturbed within the observation uncertainty which are then inverted using the TM. The resulting SD of the PO_4 ISSs are relatively large compared to the ISS values themselves, around 1–3 orders of magnitude larger than the ISS values. There are positive linear trends between the SD of observations in each grid-box and the SD of the 100 corresponding ISS estimates in each grid box (Fig. 5c). Grid-boxes with higher uncertainty in the observation results in greater uncertainty in the ISS estimates. However, two distributions can be broadly defined in Fig. 5c both with separate linear trends that correspond well with the size of the "flux out" term of the TM (see Table 1). Where the central grid-box coefficient is smaller in the TM, leading to correspondingly larger value when used in Eq. (3) (e.g. 1 – **A**), the uncertainty in ISS arising from the uncertainty in the observations is much more sensitive. This suggests that the ISS uncertainty is a function of the way the TM is constructed. The flux out term is largest in areas in our TM where convection occurs because this is where the largest transport fluxes are in the model.

4.2.2 Error from circulation estimates

Another potential source of error when inverting nutrient observations arises from the use of a modelled circulation field that will inevitably have a somewhat poorly quantified relationship to the circulation of the real ocean. Using a perturbed physics ensemble to invert our synthetic dataset, we can explore the effect of errors arising from uncertainties in circulation rates only. Figure 6a shows the mean and 1 SD of the ISS estimates generated when inverting the synthetic [PO_4] field with all 54 ensemble TMs. The values furthest from the 1 : 1 ratio line and those with the largest error bars are located in regions where convection occurs in the model (Fig. 6a and c). The strength of overturning varies within the ensemble (see Supplement) suggesting that this structural uncertainty in the model is a likely cause for the wide range of remineralisation estimates. An additional issue is that unlike most grid-boxes in our TM, where the spread of a tracer over one timestep is limited to neighbouring grid-boxes, convection

BGD
12, 4557–4593, 2015

increases the number of grid-box connections in the vertical. This could have the effect of increasing the range of remineralisation estimates because there are more grid-boxes. Figure 6b shows the same as Fig. 6a but with the convection-related values removed. Even in areas where there is no convection in the model, the range of ISS estimates from circulation uncertainty is larger relative to the range of remineralisation values. The range of errors arising from using different circulations are also larger at shallower depths compared to deeper depths in the water column (Fig. 6c and d).

To understand why different circulation estimates can have a large impact of ISSs, we explore the size of the PO_4 remineralisation flux in a grid box relative to the size of PO_4 flux from the modelled circulation. To illustrate this, we compare the steady state circulation flux of PO_4 into a grid-box with the remineralisation flux of PO_4 into each grid-box from the synthetic run. Across the whole model ocean interior, the mean proportion of remineralisation flux to the total flux into each grid box is 0.001 ± 0.015 (± 1 SD). The proportion is generally 2 magnitudes of order higher at shallower depths (290 m) than at depth (2106 m) (Fig. 7a c.f. b), reflecting the decrease in remineralisation fluxes with depth whilst circulation fluxes are generally the same magnitude (Fig. 7c and d). Even relatively small errors in the circulation flux are therefore likely to dominate over the remineralisation fluxes leading to large errors when using modelled circulation rates.

4.2.3 Error comparison

To compare the magnitude of the various possible errors, we show the global mean synthetic PO_4 remineralisation profile with the global mean and median SDs of the ISSs calculated from the ERR-OBS and ERR-CIRC experiments (Fig. 8). We use both the mean and median SD in this figure because the mean SD of the ERR-CIRC experiments are skewed by the large variability in high latitude regions (Fig. 6a). Both sources of error are larger at shallower depth and mostly decrease in magnitude with depth although the mean circulation uncertainty increases below 2000 m. The magnitude of median uncertainty from the observations is much larger than from our circulation esti-

BGD
12, 4557–4593, 2015

mates although the two are similar magnitudes when the mean SD is used to calculate profiles.

Despite similar magnitudes of uncertainty arising from both potential errors in the observations and from the model circulation field, the nature of the uncertainty is different. Uncertainty from the observations is higher in regions where observations are more uncertain, e.g. coastal areas in Fig. 5a and b, and in regions of the model where convection occurs (Fig. 5c). In contrast, the uncertainty arising from the model circulation field used will be systematic and dependent on where the model circulation is most different to the real ocean, e.g. Fig. 6. The patterns in the surface PO_4 ISSs from the MITGCM inversion are systematic which may suggest that errors are predominantly related to the ocean model (Fig. 2a) although this is less the case for the deeper ocean (Fig. 2b).

5 Inferring flux curves from remineralisation rates

5.1 Vertical profiles and dissolved organic matter

In the previous section, we have shown that a simple approach to estimating remineralisation rates using modelled transport rates is sensitive to errors. Taking the next step, in the case that remineralisation rates could be estimated with some reliability, we explore the sensitivity of inferring flux curves by vertically integrating remineralisation rates in the presence of DOM. We infer flux curves using remineralisation rates from the synthetic dataset (SYN) and a second run where no DOM is exported (SYN-NODOM). To infer a power law curve, a linear trend in fitted to the log transformed remineralisation rates following previous studies (Berelson, 2001; Lam et al., 2011; Stanley et al., 2012). The gradient of the linear trend gives the value of the exponent for the remineralisation curve, which is converted to a flux curve by adding 1 (Stanley et al., 2012; see also Fig. 1).

BGD
12, 4557–4593, 2015

The exponents from power-law curves, fitted to vertical PO_4 remineralisation profiles, when PO_4 is only exported as particulate organic matter, are all close to −1.9 (Fig. 9a). This corresponds to a flux curve exponent of −0.9, in good correspondence with −0.858 used for the run. The presence of remineralisation from DOM (see Fig. 3e) lowers the value of the fitted exponent reflecting a shallower Martin Curve (Fig. 9b). In our experiments, the remineralisation of DOM lowers the fitted exponent by as much as 0.6. This occurs because the remineralisation of DOM inflates the remineralisation rate in the shallower grid-boxes relative to those in the water column below. The fitted flux curve is shallower to reflect more remineralisation occurring at shallower depths. The DOM bias in GENIE occurs predominantly in the high latitudes where DOM is efficiently advected into the ocean interior. The range of exponents purely from this bias is of a similar magnitude and spatial distribution to the Martin Curve exponents found in Henson et al. (2012).

6 Discussion and way forward

We have presented a straightforward method of using a steady state model circulation, as represented by a transport matrix, to estimate organic matter remineralisation rates from a tracer climatology. Our main goal is to explore the feasibility of using this method to infer organic matter flux curves aiding additional understanding of the biological pump in the modern ocean. Our results show that this method is associated with a number of significant sources of error that give rise to the spatial patterns and negative values seen in an example inversion using a circulation field from a high resolution ocean model (Fig. 2). In the following sections we discuss potential directions for estimating remineralisation rates from tracer data using model circulation and considerations needed when using these to infer particle flux curves.

The sensitivity to errors in the observations is a result of the way that the transport matrix (TM) is constructed. A change in a tracer due to circulation in a model time-step is relatively localised due to the finite speed of advection and diffusion in the model

BGD
12, 4557–4593, 2015

(Khatiwala et al., 2005). Therefore, the ISS estimates are sensitive to the resulting large coefficient in the central grid-box (see Table 1). This will be a feature of all TMs constructed using the method of Khatiwala et al. (2005) regardless of resolution. Previous methods have relied on relating multiple tracers together such that the model transport terms cancel out e.g. Anderson and Sarmiento (1994); Sarmiento et al. (2002) and is a method which could be applied using the TM. The sensitivity to uncertainty in the tracer observations however, may pose a problem, especially if observational errors are different between tracers.

Our results also illustrate the sensitivity of remineralisation estimates to differences between the model transport rates and actual transport rates in the ocean. Remineralisation fluxes of PO_4 in the synthetic tracer experiments are orders of magnitude smaller than fluxes of PO_4 from circulation. Model transport rates would therefore need to attain a high level of accuracy to minimise the effect of error on the solutions (Anderson and Sarmiento, 1994; Sarmiento et al., 2002). Even a data assimilated model, such as produced by the ECCO Consortium ("Estimating the Circulation and Climate of the Ocean"; Stammer et al., 2004), designed to be a dynamically consistent estimate of ocean circulation over recent decades may still lead to large diagnosed flux errors.

The flipside of the magnitude of the circulation control on the diagnosed remineralisation rates is that tracers with a steady-state constraint, where it is expected that there should be no significant sources or sinks at depth, could be used to estimate the magnitude of the circulation-based error. As an example, we show an ISS field generated when inverting the salinity field from our synthetic dataset with the synthetic transport matrix (Fig. 10a and b). Salinity ISS are randomly distributed around zero, consistent with the concept that salinity is not increasing or decreasing in the ocean interior. In comparison, applying a different transport matrix, arbitrarily chosen from the perturbed physics ensemble, results in distinct spatial patterns in the ISSs (Fig. 10c and d). Comparing the errors from the inversion of the synthetic $[PO_4]$ field using the same TM shows that the two are visibly similar (Fig. 10e and f). This suggests that conservative tracers, i.e. tracers that do not have sources or sinks in the ocean interior

BGD
12, 4557–4593, 2015

could constrain the magnitude of error. For example, considering Eq. (3) but focussing on an individual grid-box, the ISS ($\boldsymbol{q}_{i=1}$) is a function of the TM coefficients (M_i) and the tracer concentrations (C_i) as per the example in Table 1:

$$\boldsymbol{q}_{i=1} = \sum_{i=1}^{N} M_i C_i \tag{4}$$

Redfining the modelled circulation terms to reflect that the modelled circulation is a function of a "true" circulation term and an error term ($M_i = F_i + \epsilon_i$) and substituting into Eq. (4) and expanding:

$$\boldsymbol{q}_{i=1} = \sum_{i=1}^{N} F_i C_i + \sum_{i=1}^{N} \epsilon_i C_i \tag{5}$$

For a conservative tracer at steady state, it is expected that $\sum_{i=1}^{N} F_i C_i = 0$. A significant departure from zero in $\boldsymbol{q}_{i=1}$ is likely to result from the error terms. This may provide a way forward to constrain the ISSs produced by the TM method described here. Such a method would be conceptually similar to the mixing model approaches that use steady state constraints (Gebbie and Huybers, 2010). There are however, a limited number of tracers available (e.g. temperature, salinity, δ^{18}O, Δ^{14}C, CFCs) that could realistically be used to constrain model circulation errors. In our TM, there are typically 15 grid-box connections used for each calculation which would lead to an underdetermined solution, i.e. where the unknowns outnumber the constraints. It would be interesting to see if a simplified TM with fewer coefficients, such as matching the method of Gebbie and Huybers (2010), could use this approach.

We have also shown that the remineralisation of dissolved organic matter can potentially bias the estimation of flux curves from remineralisation rate profiles. In particular, this bias, at least in our model, causes spatial variability in flux curves that is similar in pattern and magnitude to patterns of particulate organic carbon fluxes found in global

BGD
12, 4557–4593, 2015

sediment trap studies (Henson et al., 2012). Any method of estimating flux curves from estimated organic matter remineralisation rates, whether using model transport rates or using AOUR, will therefore need to take the remineralisation of DOM into account, particularly in regions where DOM is advected to deeper depths (Hansell et al., 2009). This additional source of uncertainty could be handled using other modelling approaches such as optimisation. In this approach, a biogeochemical model is set-up and optimal values of the parameters, such as the depth of remineralisation, the production of DOM and rate of DOM remineralisation, found that result in the best fit between modelled and observed nutrient fields, e.g. Kwon and Primeau (2006); Kriest et al. (2012); Teng et al. (2014). Transport matrices are a useful tool in this approach to help avoid lengthy multi-thousand year integration times for model fields to reach equilibrium (Kwon and Primeau, 2006). Given the uncertainties we have highlighted, a range of approaches may be needed to fully explore and quantify remineralisation rates and flux curves.

7 Conclusions

Spatial patterns in particulate fluxes suggest particular mechanisms that control the distribution of remineralisation in the ocean interior. Profiles of remineralisation rates derived from ocean tracers offer a potential method to estimate high resolution fields of flux curves that could supplement existing global sediment trap studies. The use of model transport rates offers one way of estimating remineralisation rates that could avoid the spatial averaging issues of combing AOU with age tracers. Through the use of a simple method using the Transport Matrix, we have shown that a high level of accuracy would be needed as remineralisation rates are an order of magnitude smaller than circulation fluxes. Aside from the errors in the observations themselves, which for the method presented were also large, the uncertainty when using modelled circulation rates is an important issue. To get information about particle fluxes, the remineralisation rates also need to be integrated vertically. This process is also associated with

BGD
12, 4557–4593, 2015

uncertainty due to the remineralisation of DOM. Both these sources of uncertainty are key issues to be considered for future approaches in quantifying the remineralisation of organic matter in the ocean interior.

The Supplement related to this article is available online at doi:10.5194/bgd-12-4557-2015-supplement.

Acknowledgements. This work was conducted as part of a project studentship (J. D. Wilson) associated with the UK Ocean Acidification Research Programme (UKOARP) grant NE/H017240/1 to A. Ridgwell and S. Barker. J. D. Wilson and A. Ridgwell acknowledge support via EU grant ERC-2013-CoG-617313. We thank Samar Khatiwala for making code and matrices available online and Julia Hargreaves for providing the ensemble data.

References

Anderson, L. A. and Sarmiento, J. L.: Redfield ratios of remineralization determined by nutrient data analysis, Global Biogeochem. Cy., 8, 65–80, doi:10.1029/93GB03318, 1994. 4561, 4574

Annan, J., Hargreaves, J., Edwards, N., and Marsh, R.: Parameter estimation in an intermediate complexity earth system model using an ensemble Kalman filter, Ocean Model., 8, 135–154, doi:10.1016/j.ocemod.2003.12.004, 2005. 4565, 4567

Archer, D. and Maier-Reimer, E.: Effect of deep-sea sedimentary calcite preservation on atmospheric CO_2 concentration, Nature, 367, 260–263, doi:10.1038/367260a0, 1994. 4560

Armstrong, R. A., Lee, C., Hedges, J. I., Honjo, S., and Wakeham, S. G.: A new, mechanistic model for organic carbon fluxes in the ocean based on the quantitative association of POC with ballast minerals, Deep-Sea Res. Pt. II, 49, 219–236, 2002. 4559

Berelson, W.: The flux of particulate organic carbon into the ocean interior: a comparison of four U.S. JGOFS regoinal studies, Oceanography, 14, 59–67, 2001. 4572

Broecker, W. S., Peacock, S. L., Walker, S., Weiss, R., Fahrbach, E., Schroeder, M., Mikolajewicz, U., Heinze, C., Key, R., Peng, T.-H., and Rubin, S.: How much deep water is formed in the

BGD
12, 4557–4593, 2015

Southern Ocean?, J. Geophys. Res.-Oceans, 103, 15833–15843, doi:10.1029/98JC00248, 1998. 4561
Deutsch, C., Sarmiento, J. L., Sigman, D. M., Gruber, N., and Dunne, J. P.: Spatial coupling of nitrogen inputs and losses in the ocean, Nature, 445, 163–167, doi:10.1038/nature05392, 2007. 4562
Dietze, H. and Oschlies, A.: Modeling abiotic production of apparent oxygen utilisation in the oligotrophic subtropical North Atlantic, Ocean Dynam., 55, 28–33, 2005. 4566
Duteil, O., Koeve, W., Oschlies, A., Bianchi, D., Galbraith, E., Kriest, I., and Matear, R.: A novel estimate of ocean oxygen utilisation points to a reduced rate of respiration in the ocean interior, Biogeosciences, 10, 7723–7738, doi:10.5194/bg-10-7723-2013, 2013. 4566
Edwards, N. and Marsh, R.: Uncertainties due to transport-parameter sensitivity in an efficient 3-D ocean-climate model, Clim. Dynam., 24, 415–433, 2005. 4564
Feely, R., Sabine, C., Schlitzer, R., Bullister, J., Mecking, S., and Greely, D.: Oxygen utilization and organic carbon remineralization in the upper water column of the Pacific Ocean, J. Oceanogr., 60, 45–52, 2004. 4560
Garcia, H., Locarnini, R., Boyer, T., Antonov, J., Zweng, M., Baranova, O., and Johnson, D.: World Ocean Atlas 2009, Volume 4: Nutrients (phosphate, nitrate, silicate), in: NOAA Atlas NESDIS 71, edited by: Levitus, S., U.S. Government Printing Office, Washington, DC, 398 pp., 2010. 4563, 4567, 4569, 4588
Gebbie, G. and Huybers, P.: Total matrix intercomparison: a method for determining the geometry of water-mass pathways, J. Phys. Oceanogr., 40, 1710–1728, doi:10.1175/2010JPO4272.1, 2010. 4561, 4575
Hansell, D., Carlson, C., Repeta, D., and Schlitzer, R.: Dissolved organic matter in the ocean: a controversy stimulates new insights, Oceanography, 22, 202–211, 2009. 4576
Henson, S., Sanders, R., and Madsen, E.: Global patterns in efficiency of particulate organic carbon export and transfer to the deep ocean, Global Biogeochem. Cy., 26, GB1028, doi:10.1029/2011GB004099, 2012. 4559, 4573, 4576, 4584
Henson, S. A., Sanders, R., Madsen, E., Morris, P. J., Le Moigne, F., and Quartly, G. D.: A reduced estimate of the strength of the ocean's biological carbon pump, Geophys. Res. Lett., 38, L04606, doi:10.1029/2011GL046735, 2011. 4561, 4563
Honjo, S., Manganini, S. J., Krishfield, R. A., and Francois, R.: Particulate organic carbon fluxes to the ocean interior and factors controlling the biological pump: a syn-

BGD
12, 4557–4593, 2015

thesis of global sediment trap programs since 1983, Prog. Oceanogr., 76, 217–285, doi:10.1016/j.pocean.2007.11.003, 2008. 4559
Honjo, S., Eglinton, T., Taylor, C., Ulmer, K., Sievert, S., Bracher, A., German, C., Edgcomb, V., Francois, R., Iglesias-Rodriguez, M., Van Mooy, B., and Repeta, D.: Understanding the role of the biological pump in the global carbon cycle: an imperative for ocean science, Oceanography, 27, 10–16, 2014. 4559
Ito, T., Follows, M. J., and Boyle, E. A.: Is AOU a good measure of respiration in the oceans?, Geophys. Res. Lett., 31, L17305, doi:10.1029/2004GL020900, 2004. 4566
Jenkins, W. J.: Oxygen utilization rates in North Atlantic subtropical gyre and primary production in oligotrophic systems, Nature, 300, 246–248, doi:10.1038/300246a0, 1982. 4560
Jin, X., Gruber, N., Dunne, J. P., Sarmiento, J. L., and Armstrong, R. A.: Diagnosing the contribution of phytoplankton functional groups to the production and export of particulate organic carbon, $CaCO_3$, and opal from global nutrient and alkalinity distributions, Global Biogeochem. Cy., 20, GB2015, doi:10.1029/2005GB002532, 2006. 4561
Khatiwala, S.: A computational framework for simulation of biogeochemical tracers in the ocean, Global Biogeochem. Cy., 21, GB3001, doi:10.1029/2007GB002923, 2007. 4562, 4565
Khatiwala, S., Visbeck, M., and Cane, M. A.: Accelerated simulation of passive tracers in ocean circulation models, Ocean Model., 9, 51–69, doi:10.1016/j.ocemod.2004.04.002, 2005. 4562, 4565, 4574
Klaas, C. and Archer, D. E.: Association of sinking organic matter with various types of mineral ballast in the deep sea: implications for the rain ratio, Global Biogeochem. Cy., 16, 1116, doi:10.1029/2001GB001765, 2002. 4559
Kriest, I., Oschlies, A., and Khatiwala, S.: Sensitivity analysis of simple global marine biogeochemical models, Global Biogeochem. Cy., 26, GB2029, doi:10.1029/2011GB004072, 2012. 4576
Kwon, E. Y. and Primeau, F.: Optimization and sensitivity study of a biogeochemistry ocean model using an implicit solver and in situ phosphate data, Global Biogeochem. Cy., 20, GB4009, doi:10.1029/2005GB002631, 2006. 4576
Kwon, E. Y., Primeau, F., and Sarmiento, J. L.: The impact of remineralization depth on the air-sea carbon balance, Nat. Geosci., 2, 630–635, doi:10.1038/ngeo612, 2009. 4559
Lam, P. J., Doney, S. C., and Bishop, J. K. B.: The dynamic ocean biological pump: insights from a global compilation of particulate organic carbon, $CaCO_3$, and opal concentration profiles

BGD
12, 4557–4593, 2015

from the mesopelagic, Global Biogeochem. Cy., 25, GB3009, doi:10.1029/2010GB003868, 2011. 4559, 4572

Le Moigne, F. A. C., Sanders, R. J., Villa-Alfageme, M., Martin, A. P., Pabortsava, K., Planquette, H., Morris, P. J., and Thomalla, S. J.: On the proportion of ballast versus non-ballast associated carbon export in the surface ocean, Geophys. Res. Lett., 39, L15610, doi:10.1029/2012GL052980, 2012. 4559

Lutz, M., Caldeira, K., Dunbar, R., and Behrenfeld, M.: Seasonal rhythms of net primary production and particulate organic carbon flux to depth describe the efficiency of biological pump in the global ocean, J. Geophys. Res.-Oceans, 112, C10011, doi:10.1029/2006JC003706, 2007. 4559

Marsay, C. M., Sanders, R. J., Henson, S. A., Pabortsava, K., Achterberg, E. P., and Lampitt, R. S.: Attenuation of sinking particulate organic carbon flux through the mesopelagic ocean, P. Natl. Acad. Sci. USA, 112, 1089–1094, doi:10.1073/pnas.1415311112, 2015. 4559

Martin, J., Knauer, G., Karl, D. M., and Broenkow, W.: VERTEX: carbon cycling in the northeast Pacific, Deep-Sea Res., 43, 267–285, 1987. 4559

Passow, U.: Switching perspectives: do mineral fluxes determine particulate organic carbon fluxes or vice versa?, Geochem. Geophy. Geosy., 5, Q04002, doi:10.1029/2003GC000670, 2004. 4559

Ridgwell, A., Hargreaves, J. C., Edwards, N. R., Annan, J. D., Lenton, T. M., Marsh, R., Yool, A., and Watson, A.: Marine geochemical data assimilation in an efficient Earth System Model of global biogeochemical cycling, Biogeosciences, 4, 87–104, doi:10.5194/bg-4-87-2007, 2007a. 4564, 4565, 4566, 4567

Ridgwell, A., Zondervan, I., Hargreaves, J. C., Bijma, J., and Lenton, T. M.: Assessing the potential long-term increase of oceanic fossil fuel CO_2 uptake due to CO_2-calcification feedback, Biogeosciences, 4, 481–492, doi:10.5194/bg-4-481-2007, 2007b. 4565, 4566, 4567

Roth, R., Ritz, S. P., and Joos, F.: Burial-nutrient feedbacks amplify the sensitivity of atmospheric carbon dioxide to changes in organic matter remineralisation, Earth Syst. Dynam., 5, 321–343, doi:10.5194/esd-5-321-2014, 2014. 4560

Sarmiento, J., Gruber, N., Brzezinski, M., and Dunne, J.: High-latitude controls of thermocline nutrients and low latitude biological productivity, Nature, 427, 56–60, doi:10.1038/nature02127, 2004. 4561

BGD
12, 4557–4593, 2015

Sarmiento, J. L., Dunne, J., Gnanadesikan, A., Key, R. M., Matsumoto, K., and Slater, R.: A new estimate of the $CaCO_3$ to organic carbon export ratio, Global Biogeochem. Cy., 16, 54-1–54-12, doi:10.1029/2002GB001919, 2002. 4561, 4574

Sonnerup, R. E., Mecking, S., and Bullister, J. L.: Transit time distributions and oxygen utilization rates in the Northeast Pacific Ocean from chlorofluorocarbons and sulfur hexafluoride, Deep-Sea Res. Pt. I, 72, 61–71, doi:10.1016/j.dsr.2012.10.013, 2013. 4561

Stammer, D., Ueyoshi, K., Köhl, A., Large, W. G., Josey, S. A., and Wunsch, C.: Estimating air-sea fluxes of heat, freshwater, and momentum through global ocean data assimilation, J. Geophys. Res.-Oceans, 109, C05023, doi:10.1029/2003JC002082, 2004. 4574

Stanley, R. H. R., Doney, S. C., Jenkins, W. J., and Lott, III, D. E.: Apparent oxygen utilization rates calculated from tritium and helium-3 profiles at the Bermuda Atlantic Time-series Study site, Biogeosciences, 9, 1969–1983, doi:10.5194/bg-9-1969-2012, 2012. 4561, 4572

Teng, Y.-C., Primeau, F., Moore, J., Lomas, M., and Martiny, A.: Global-scale variations of the ratios of carbon to phosphorus in exported marine organic matter, Nat. Geosci., 7, 895–898, doi:10.1038/ngeo2303, 2014. 4576

Wilson, J. D., Barker, S., and Ridgwell, A.: Assessment of the spatial variability in particulate organic matter and mineral sinking fluxes in the ocean interior: implications for the ballast hypothesis, Global Biogeochem. Cy., 26, GB4011, doi:10.1029/2012GB004398, 2012. 4559

Zeebe, R. E.: LOSCAR: Long-term Ocean-atmosphere-Sediment CArbon cycle Reservoir Model v2.0.4, Geosci. Model Dev., 5, 149–166, doi:10.5194/gmd-5-149-2012, 2012. 4562

BGD
12, 4557–4593, 2015

Table 1. Example of using a transport matrix to calculate PO_4 remineralisation ($\mu mol\,kg^{-1}\,dt^{-1}$) in one grid-box from PO_4 concentrations ($\mu mol\,kg^{-1}$) given in ***c***. Grid-boxes are arbitrarily numbered, where the 1 is the grid-box where the calculation is taking place. Coefficients from **A** represent the change in a tracer due to circulation after a single time-step, e.g. the proportion of tracer concentration left in grid-box 1 after one time step is 0.98753 (see Eq. 1). Coefficients from **A** – **I** are the same except now grid-box 1 is equivalent to 1–0.98753 (see Eq. 2). The sum of the coefficients are shown underneath. The amount in italics is the estimated remineralisation combining **A** – **I** and ***c*** (***q*** in Eq. 3).

Grid-Box	**A**	**A** – **I**	***c***
1 ("flux out")	0.98753	−0.01247	2.42
2	−0.00015	−0.00015	2.37
3	0.01113	0.01113	2.42
4	0.00002	0.00002	2.37
5	0.00008	0.00008	2.37
6	−0.00001	−0.00001	2.38
7	0.00006	0.00006	2.36
8	0.00132	0.00132	2.41
	1.00000	-2.38×10^{-7}	1.35×10^{-5}

BGD
12, 4557–4593, 2015

Table 2. Simulations and experiments used in this paper.

Name	Description
Synthetic Datasets	
SYN	A synthetic [PO_4] dataset derived from a 10 000 year spin-up of GENIE. A corresponding transport matrix is diagnosed.
SYN-NODOM	As the SYN dataset but with the fraction of DOM exported set to zero.
Experiments	
TWIN	The synthetic [PO_4] field is inverted using the TM and compared to the modelled [PO_4] remineralisation from SYN
ERR-DOM	Particulate flux curves are estimated from the PO_4 remineralisation rates from the SYN and SYN-NODOM datasets.
ERR-OBS	The synthetic [PO_4] is perturbed with error estimates from World Ocean Atlas observations
ERR-CIRC	The synthetic [PO_4] is inverted using 54 TMs diagnosed from a perturbed-physics ensemble.

BGD
12, 4557–4593, 2015

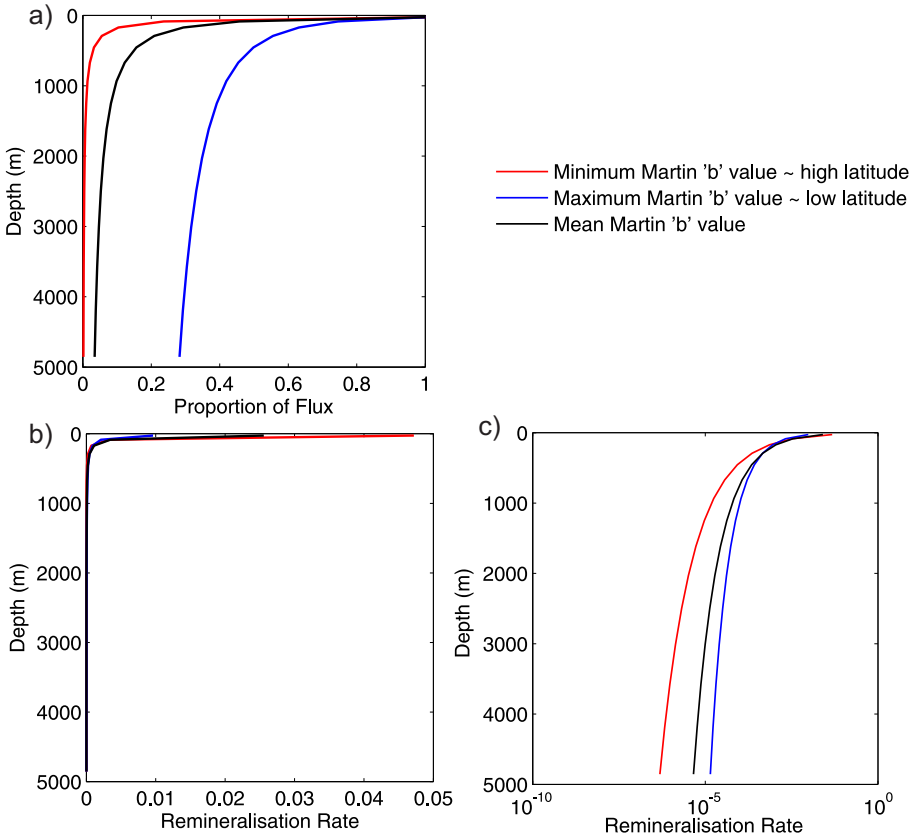

Figure 1. The range of observed Martin Curves and associated remineralisation rate profiles. **(a)** The mean ($b = -0.639$) and global range ($b = -1.18$ to -0.24) of Martin Curves found by Henson et al. (2012) calculated for a unit flux and export depth (z_0) via $F_z = 1 \cdot \frac{z}{z_0}^{-b}$. **(b)** The first derivativee of each flux curve in panel **(a)**, equivalent to a vertical profile of organic matter remineralisation calculated as $\frac{dF_z}{dz} = \frac{-b}{z_0} \cdot \frac{z}{z_0}^{-(b-1)}$.

BGD
12, 4557–4593, 2015

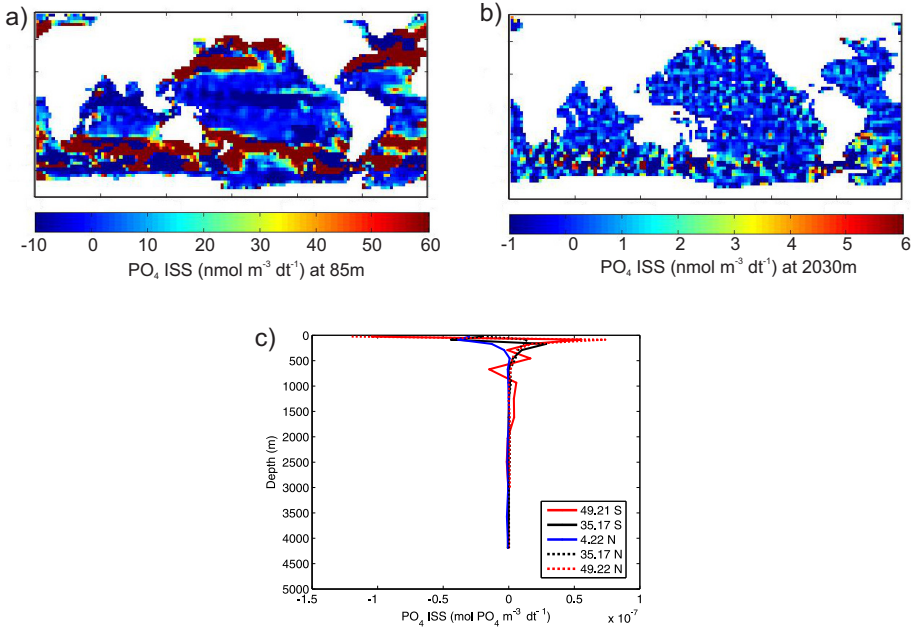

Figure 2. Example of using a GCM transport matrix to estimate PO_4 remineralisation rates. **(a)** The estimated PO_4 remineralisation rates generated using the MIT GCM transport matrix at 85 m and **(b)** 2030 m. **(c)** Vertical profiles of PO_4 remineralisation rates estimated using transport rates from an MITGCM transport matrix (equivalent to Fig. 1b) are shown from latitudes corresponding to equivalent regions in the Pacific at 223° E.

BGD
12, 4557–4593, 2015

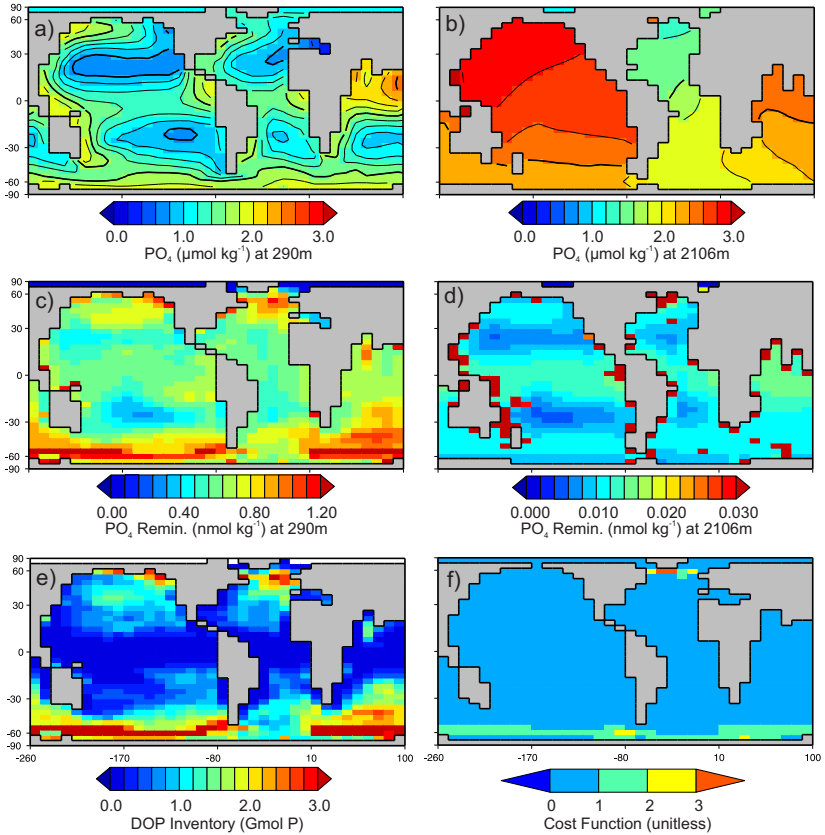

Figure 3. The synthetic tracer dataset used for transport matrix inversions. **(a)** $[PO_4]$ ($\mu mol\,kg^{-1}$) at 290 m and **(b)** 2106 m. **(c)** The total annual remineralisation flux of PO_4 ($nmol\,kg^{-1}\,dt^{-1}$) at 290 m and **(d)** 2106 m. **(e)** The water column integrated inventory of phosphorus in dissolved organic matter in the ocean interior (mol P). **(f)** A cost function for convection occurring in a water column in one model year (unitless). Higher values indicate stronger convection in the model.

BGD
12, 4557–4593, 2015

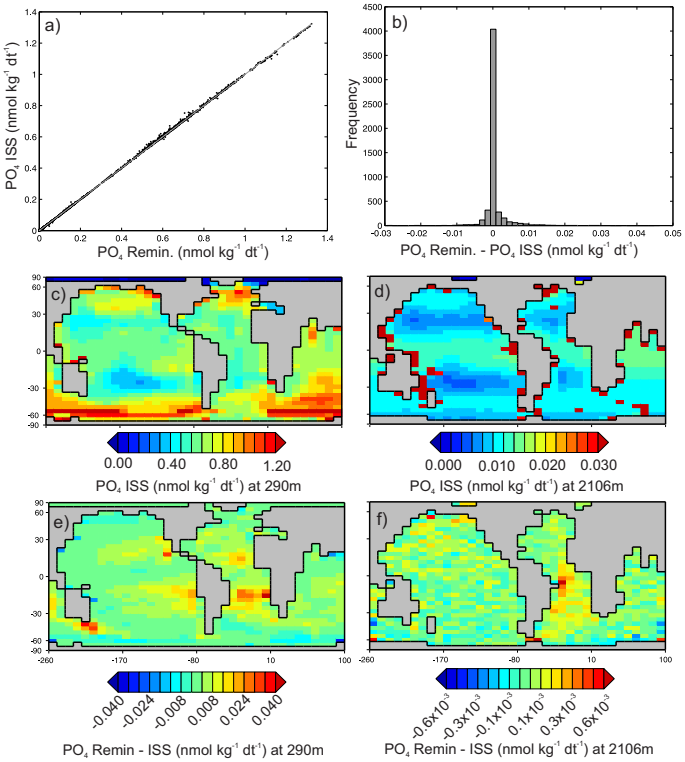

Figure 4. Results from inverting the synthetic dataset with its corresponding transport matrix. **(a)** The interior source/sink estimate for PO_4 when inverting the synthetic [PO_4] field with the corresponding transport matrix vs. the synthetic PO_4 remineralisation with a 1 : 1 ratio line, **(b)** the distribution of errors for the PO_4 interior source/sink estimates (50 bins sized 0.15×10^{-5}). **(c)** The interior source/sink estimate for PO_4 at 290 m and **(d)** 2106 m. **(e)** Difference between inverse interior source/sink estimates and the synthetic remineralisation field at 290 m and **(f)** 2106 m.

BGD
12, 4557–4593, 2015

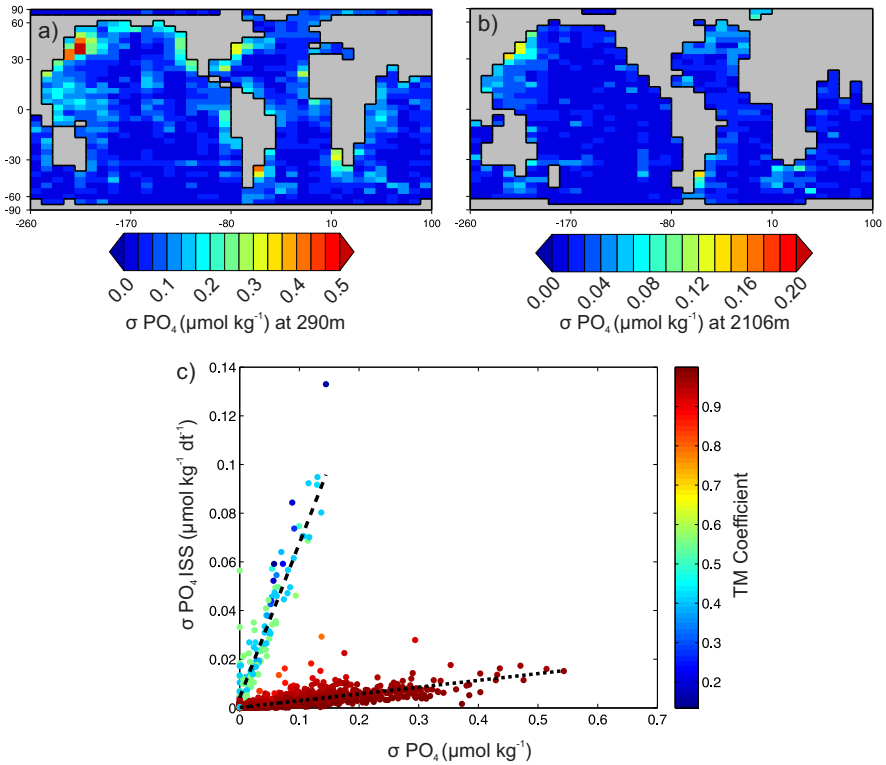

Figure 5. Assessment of the errors arising from the uncertainty in [PO_4] observations. **(a)** The SD of [PO_4] from the World Ocean Atlas 2009 (Garcia et al., 2010) 1° climatology regridded to the GENIE grid at 290 m and **(b)** 2106 m. **(c)** SD of all PO_4 interior source/sink estimates when the synthetic [PO_4] field is randomly perturbed within a normal distribution given by the SD of observations. The two distributions are distinguished by the value of the TM coefficient in the same grid-box shown by the colour bar. A linear regression trend line fitted to data where the coefficient is > 0.8 (dotted line) gives a slope of 0.03 (R^2 = 0.71). When fitted to data < 0.8 (dashed line), the slope is 0.63 (R^2 = 0.84).

BGD
12, 4557–4593, 2015

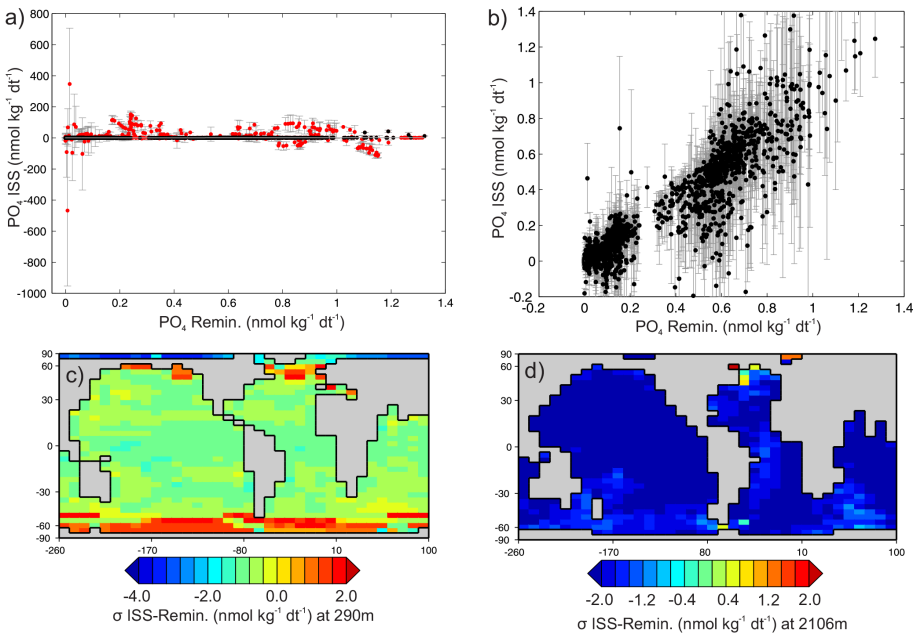

Figure 6. Assessment of error arising from using circulation estimates. **(a)** Comparison of ISS estimates for each grid-box from the 54 ensemble members against the synthetic dataset remineralisation. Error bars are 1 SD around the mean. Red values indicate regions with convection. **(b)** As panel **(a)** but with the red values removed. Note the difference in scale. **(c)** The SD of PO_4 ISS errors (Model – ISS) in $\mu mol\,kg^{-1}\,dt^{-1}$ for 290 m. Values are shown on a log scale. **(d)** As panel **(c)** but at 2106 m.

BGD
12, 4557–4593, 2015

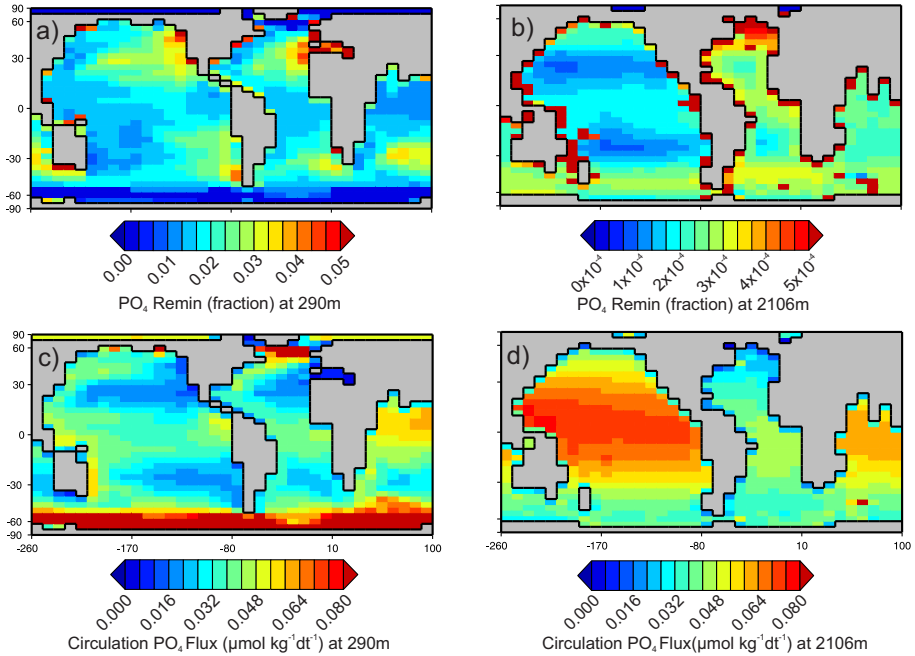

Figure 7. Comparison of inputs of PO_4 from remineralisation and circulation at steady-state. **(a)** PO_4 remineralisation as a proportion of the total PO_4 flux into each grid-box calculated using the synthetic tracer field at 290 m and **(b)** 2106 m. **(c)** The flux of PO_4 into each grid-box from circulation only ($\mu mol\,kg^{-1}\,dt^{-1}$) from the synthetic tracer fields at 290 m and **(d)** 2106 m.

BGD
12, 4557–4593, 2015

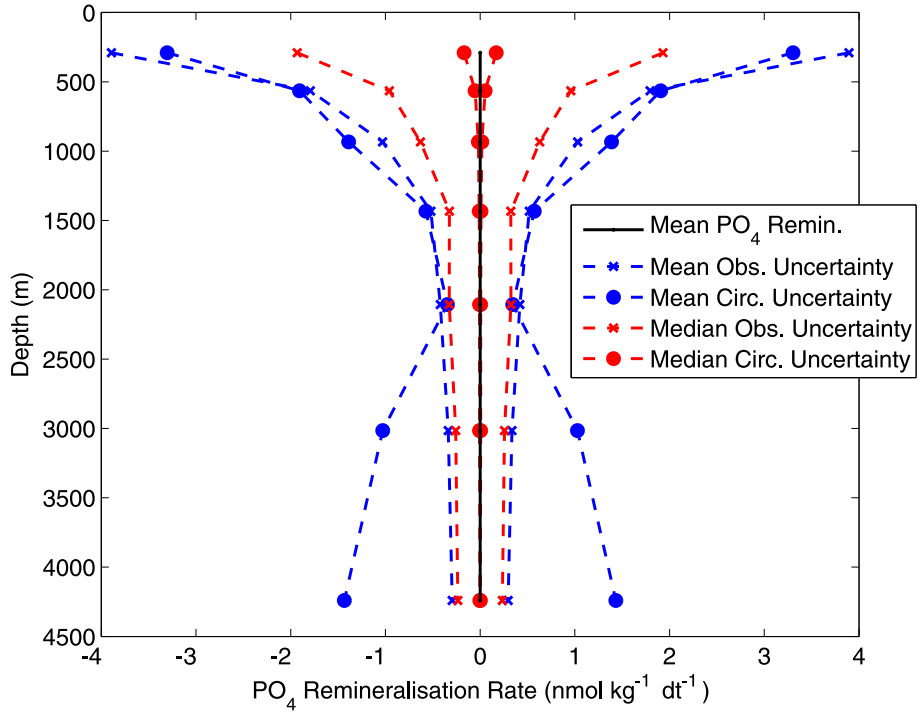

Figure 8. Comparison of error magnitudes when estimating remineralisation rates. The global mean PO_4 remineralisation profile from the synthetic dataset is shown with the plus and minus the mean and median SDs from the ERR-OBS and ERR-CIRC experiments.

BGD
12, 4557–4593, 2015

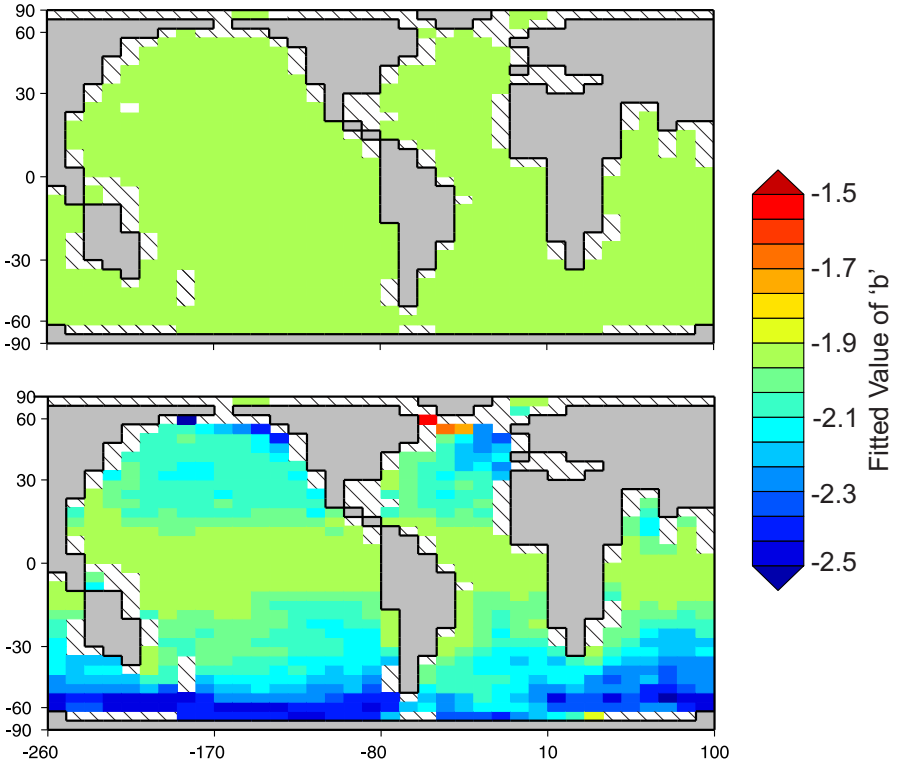

Figure 9. Assessment of the uncertainty associated with dissolved organic matter when inferring flux profiles. Value of the exponent when fitting a power law to the water column remineralisation rates from **(a)** a model with remineralisation from only sinking particulate and **(b)** a model with particulate and dissolved organic matter. A value of −0.858 for the Martin Curve was used in both models. All curves were fitted with an $R^2 > 0.9$. The exponent for the remineralisation curve is equivalent to -0.858 ± 1. More negative values indicate a Martin Curve that predicts shallower remineralisation in the water column. Hatched areas indicate where the water column contained too few boxes to fit a remineralisation curve ($n < 3$).

BGD
12, 4557–4593, 2015

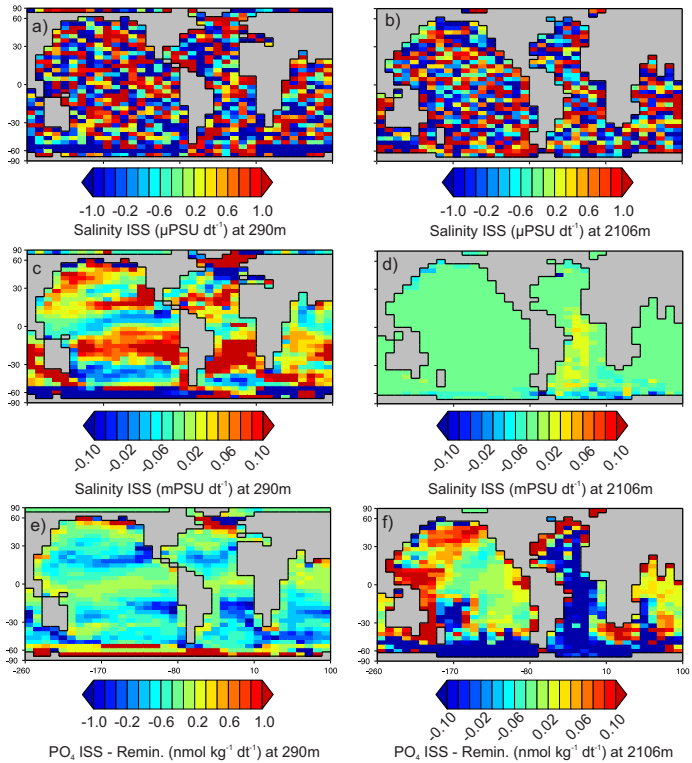

Figure 10. Inversion of salinity as a possible constraint on the uncertainty from using a modelled circulation. **(a)** Inversion of the salinity field from the synthetic dataset using the corresponding transport matrix at 290 m (PSU dt^{-1}) and at **(b)** 2106 m. **(c)** Inversion of the salinity field using a alternative transport matrix from the perturbed-physics ensemble (PSU dt^{-1}) at 290 m and **(d)** 2106 m. **(e)** The error of the synthetic PO_4 ISS ($\mu mol\,kg^{-1}\,dt^{-1}$) (ISS-synthetic) using the same transport matrix in panels **(c, d)** at 290 m and **(f)** 2106 m.

BGD
12, 4557–4593, 2015